# AN IMPROVED HARMONIC REDUCTION TECHNIQUE FOR THE PV-WIND HYBRID GENERATION SCHEME USING MODIFIED WHALE OPTIMIZATION ALGORITHM (MWOA)

Swati SUMAN[1]*, Debashis CHATTERJEE[2], Mukul ANAND[3], Rupali MOHANTY[4], Anagha BHATTACHARYA[5]

*This paper contributes to the field of power quality by using MWOA search based SHEPWM application for a microgrid system. Generally, large number of switching angles are used to remove harmonics, but higher-order harmonics are left unattended, increasing the switching losses and reducing system efficiency. Here, both lower and higher orders are suppressed with just five switching angles. These angles give equivalently good results as the seven, but with reduced losses. Amongst all MWOA works best as THD achieved was only 1.6% suitable for practical applications. It was executed in MATLAB2016b and an experimental setup was developed to justify the results.*

**Keywords**: Harmonic analysis; Selective Harmonic Elimination Pulse Width Modulation (SHEPWM) inverters; Metaheuristic techniques

## 1. Introduction

In recent years, renewable sources of electricity have been gaining increased importance. The clean and green features are what are making these resources popular. Solar and wind power have additional advantages in that they are both readily available and free [1].

The choice of a proper converter is necessarily important for feeding the power grid. Multilevel converters can efficiently convert DC to AC [2]. There are many PWM techniques adopted, such as Sinusoidal Pulse Width Modulation (SPWM), Space Vector PWM (SVPWM), and SHEPWM for the same. It has been reported that the Total Harmonic Distortion (THD) of SPWM**,** was approximately 40%, which is considered significant in terms of maintaining power quality. Power quality was maintained by using a static var compensator [3]. Several articles discuss the attractive features of the SHEPWM inverter. It has

[1] JADAVPUR UNIVERSITY, India, e-mail: swati.sep@gmail.com
[2] JADAVPUR UNIVERSITY, India, e-mail: debashisju@yahoo.com
[3] India, e-mail: mukulanand.anand209@gmail.com
[4] India, e-mail: rups.mohanty25@gmail.com
[5] India, e-mail: anaghabhattacharya@gmail.com

decreased switching and conversion losses, better electromagnetic interference (EMI), etc. Therefore, SHEPWM is considered a good option in terms of higher power applications and has also been used in the present paper. It eliminates "d-1" of lower order harmonics with "d" of triggering angles [4]. To achieve this, the solving of non-linear equations was difficult using the Gauss-Newton Raphson method [5]. To solve a higher degree polynomial equation, this method would increase the computation time and complexity and decrease the convergence speed.

There are many optimization techniques adopted to solve the problems. These evolutionary techniques are appropriately suited depending upon the problem statement. A detailed discussion of the wind-penetrated microgrid system has been discussed [6]. DFIG operations at sub and super synchronous speeds and their control have been discussed in detail [7-9]. A control technique using a piecewise-mixed model for storing angles offline has been described [19].

BBO based SHEPWM technique, [10] in a DFIG connected microgrid system. A comparison with several other search-based algorithms such as Particle Swarm Optimization (PSO), Cuckoo Search Algorithm (CSA), etc., has been performed in which BBO performed better. In [11], the Grey Wolf Optimization (GWO) technique is used in the hybrid system to solve the real and reactive power problems. A modified grey wolf optimization technique has been used in the hybrid cascaded multilevel inverter for harmonic reduction [12]. MPP was tracked using the bacterial foraging method [13]. WOA has been thoroughly discussed in [14, 15] for a variety of engineering field applications. A comparative analysis of different optimization algorithms has been executed in standalone systems [16]. Later, [17] introduced a modified whale optimization technique for solar parameter identification. [18] has used an adaptive genetic algorithm technique to track the MPPT in a PV system.

A modified whale optimization technique has been used in the present technique as its usage for harmonic reduction is not noted much in the literature for hybrid systems. The MWOA is superior when compared to PSO, GWO, and BBO. The use of objective functions in the MWOA easily reduces both higher and lower order harmonics, which was a limitation in the simple SHEPWM technique. The adopted modified WOA-based optimized SHEPWM control technique has easier implementation and faster convergence in the hybrid microgrid connected system, which marks the novelty of the paper. Standard reports have been used for comparison [20,21] in the present paper. The hardware results are also included to justify their applications in the practical scenario.

The paper has been presented in the following sections. Section 2 discusses the proposed scheme, Section 3 comprises the harmonic elimination technique in detail, Section 4 presents the whale optimization technique, Section 5 presents the PV-wind characteristics equations, and Section 6 deals with the simulation and

hardware results with various comparison tables, and last of all, conclusion is discussed in Section 7.

## 2. Proposed Scheme

The proposed model is illustrated in Fig. 1. Generally, the microgrid is powered by a distributed storage system or generators. Contrary to that, a hybrid source of PV and wind has been introduced here. The stator is coupled with the microgrid at a frequency of 50 Hz. The direction of the wind tends to rotate the wind turbine. The turbine is accountable for the pitch angle control, which adjusts the speed for the blade's protection. The induction generator is directly coupled to the gearbox.

As shown in Fig. 1, there are two types of converters used in the process: rotor-side converters (RSC) and grid-side converters (GSC). RSC is directly connected to the IG rotor, whereas GSC, as the name says, is connected to the grid.

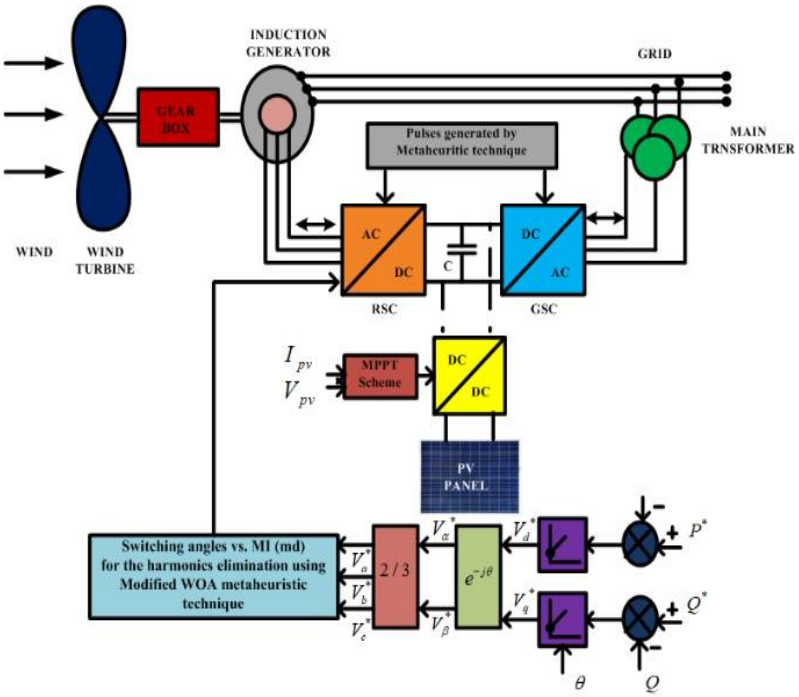


Fig. 1. Proposed model

When the wind speed is high, the DFIG will operate in a super-synchronous mode, and when the wind speed is low, it will operate in a sub-synchronous mode. In the latter part, active power is given to the rotor from the DC bus and vice-versa. At the time of sub-synchronous mode, PV with a DC-DC

boost converter supports and helps to maintain the voltage dip. The MPPT controller helps track the maximum power. Perturb and Observe (P & O) has been used in this regard. Conventional control strategies, converters, and non-linear loads all produce harmonics, thus leading to major power quality issues. This leads to an extensive need for harmonic compensation. The back-to-back converters use an optimized SHEPWM technique that helps to deal with the harmonics. It works at a low frequency to avoid switching losses, thus making the system more competent. The SHEPWM technique uses the MWOA technique.

The angles found are given to the lookup table for offline usage. The five switching angles produce equivalently good results as seven switches, but with fewer switching losses, thus improving the system efficiency. A comparison with other search-based techniques was carried out, but MWOA solves the purpose more efficiently and gives a satisfactory result.

## 3. SHEPWM application in converters for harmonic analysis

The output voltage, shown in Fig. 2, can be illustrated in terms of the Fourier series. According to the quarter-wave symmetry, only odd harmonics are present, i.e., ($a_n$=0).

$$v(wt) = \sum_{n=1}^{\infty} (a_n \cos nwt + b_n \sin nwt) \tag{1}$$

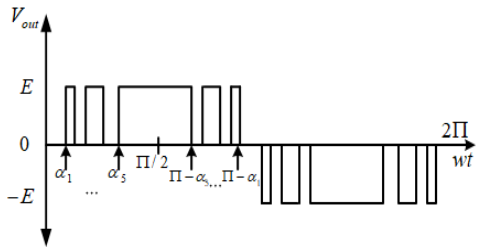


Fig. 2. The voltage waveform of unipolar SHEPWM inverter

where

$$b_n = -\frac{4}{n\pi} \sum_{d=1}^{m} (-1)^d \cos n\alpha_d \tag{2}$$

On expanding equation (2a) we get,

$$b_1 = \cos\alpha_1 - \cos\alpha_2 + \cos\alpha_3 - \cos\alpha_4 + \cos\alpha_5 = M \tag{2a}$$
$$b_5 = \cos 5\alpha_1 - \cos 5\alpha_2 + \cos 5\alpha_3 - \cos 5\alpha_4 + \cos 5\alpha_5 = 0$$
$$b_7 = \cos 7\alpha_1 - \cos 7\alpha_2 + \cos 7\alpha_3 - \cos 7\alpha_4 + \cos 7\alpha_5 = 0$$
$$b_{29} = \cos 29\alpha_1 - \cos 29\alpha_2 + \cos 29\alpha_3 - \cos 29\alpha_4 + \cos 29\alpha_5 = 0$$

The objective function can be given as

$$y(\alpha) = (b_1 - M)^2 + K_{17} * (b_{17} - e_{17})^2 + ... + K_n * (b_n - e_n)^2 \quad (3)$$

Subjected to

$$0 < \alpha_1 < \alpha_2 .... < \alpha_m < \Pi/2 \quad (4)$$

where, $n$ is the harmonic order; $\alpha_1 .... \alpha_d$ are the five triggering angles; y is the objective function; e is a value close to zero, so that the harmonics value should be close to it; k is known as the priority setter value, because it prioritizes the harmonic that is too high and urgently needs to be reduced; $b_1$, $b_5$, $b_7$... bn= amplitude of harmonic voltage., in the case of line-to-line voltage triple-n and the even harmonics are non-existent.

The fundamental component was adjusted within the range set for the modulation index. Lower order harmonics such as $b_1$, $b_5$, b7... were removed by finding the five numbers of triggering angles. These angles were calculated by $b_5$, $b_7$, b11, and b13, equating the non-linear equations to zero. If the switching angles are considered to be of a 'd' number, then it is efficient enough to remove the '(d-1)' number of harmonics. Generally, odd harmonics are present, and even harmonics are mostly zero. In the present case, five switching angles were found which dealt with the lower order harmonics such as $5^{th}$, $7^{th}$, $11^{th}$, and $13^{th}$, and the rest of the higher-order harmonics were controlled by the objective function in equation (3) by following the condition mentioned in equation (4). In the present case, harmonics of up to twenty-nine were taken into consideration. On considering an odd number of switching angles, such as three, the harmonics such as the 5th and 7th were removed. Similarly, by considering an even number of switching angles like four, the harmonics of the $5^{th}$, $7^{th}$, and $11^{th}$ would be mitigated. So, the advantage is that by using the least number of triggering angles, a wider number of harmonics can be removed, as that would decrease the switching losses and would increase the performance capability and efficiency of the system. By using equations (2), (3), and (5) in the search-based algorithm, the minimum THD possible was generated with corresponding angles, which were further considered. As shown later, the harmonics up to the $29^{th}$ order were decreased with five triggering pulses, reducing the switching losses. This limits the use of a higher number of triggering pulses and maintains the efficiency of the system.

$$\%THD = \sqrt{\frac{b_5^2 + b_7^2 + ... + b_n^2}{b_1^2}} \quad (5)$$

## 4. Whale Optimization Algorithm

WOA is a swarm-based optimizing technique that is motivated by how the whale hunts. Its implementation is easier, and it has superior performance over many other complex evolutionary techniques. It has only one controlling parameter, i.e., the time, which is to be tuned finely. Humpback whales search for their food in a multidimensional search space. The algorithm is very similar to grey wolf optimization (GWO). The location of these whales is considered a decision, whereas the distance between the whales and the food can be denoted as an objective function. The hunt for food involves three steps, as follows:

a) *Encircling the prey:* The whales forage for and surround their prey. Initially, the optimal design is unknown, so the current best solution is considered the target prey or close to the optimum solution. Meanwhile, the search for the supreme search agent continues so that the other search agents update their positions near to it. It can be expressed by equations:

$$\vec{D} = \left|\vec{C}.\overrightarrow{X^*}(t) - \vec{X}(t)\right| \qquad \vec{X}(t+1) = \overrightarrow{X^*}(t) - \vec{A}.\vec{D} \tag{6, 7}$$

$$\vec{A} = 2\vec{a}.\vec{r_1} - \vec{a} \tag{8}$$

$$\vec{C} = 2\vec{r_2} \tag{9}$$

where, $\vec{A}$ and $\vec{C}$ coefficient vectors, t refers to the present iteration, $\overrightarrow{X^*}$ is the position of the prey, and $\vec{x}$ is the position of the whale. '.' is the element-by-element multiplication and || is the absolute value, $\vec{a}$ decreases from 2 to 0 in each iteration, $\vec{r_1}$ and $\vec{r_2}$ are taken as random vectors in [0, 1].

b) *Bubble-Net attacking Method (Exploitation phase):* It is bifurcated into two steps:

i) *Shrinkage of the encircling mechanism:* This is accomplished by lowering the value of $\vec{a}$. The updated current position was achieved by the previous position and obtained the best position.

ii) *Spiral updating position:* When whales approach their prey, they produce bubbles in a spiral pattern. They do this to compute the distance between them and the prey, which forms a spiral shape which is denoted as $\vec{D}'$.

$$\vec{X}(t+1) = \vec{D}'.e^{bl}.\cos(2\Pi l) + \overrightarrow{X^*}(t) \tag{10}$$

$$\vec{X}(t+1) = \overrightarrow{X^*}(t) - \vec{A}.\vec{D} \quad \text{if } p<0.5 \tag{11}$$

$$\vec{X}(t+1) = \vec{D}'.e^{bl}.\cos(2\Pi l) + \overrightarrow{X^*}(t) \text{ if } p>=0.5 \tag{12}$$

where l is the arbitrary value between [-1,1], b is the fix coefficient of the spiral shape, and p is the probability parameter.

a) *Searching for prey (Exploration phase):* $\vec{A}$ is considered responsible for the exploration of the search for the prey and $\overrightarrow{X_{rand}}$ is the current spot of the whale arbitrarily taken from the whale population. If $|\vec{A}|$<=1 the whales will approach the prey (exploitation) and if $|\vec{A}|$>1 the whales will not update their position based on the best solution but will choose a random whale as the best position (exploitation). It is given in the equations below:

$$\vec{D} = \left|\vec{C}.\overrightarrow{X_{rand}} - \vec{X}\right| \tag{13}$$

$$\vec{X}(t+1) = \overrightarrow{X_{rand}} - \vec{X}.\vec{D} \tag{14}$$

### 4.1 The Proposed Compensation technique using MGWO

Some of the limitations of WOA have compelled the authors to develop MWOA. For the exploration and exploitation phases, mostly the values are based on randomization, which would increase the computational complexity and time for the complex problems. As it has been mentioned earlier, it depends on one parameter i.e., $\vec{a}$, which decreases the convergence speed. Some of the limitations of WOA have compelled the authors to develop MWOA. For the exploration and exploitation phases, mostly the values are based on randomization, which would increase the computational complexity and time for the complex problems. As it has been mentioned earlier, it depends on one parameter i.e., $\vec{a}$, which is which decreases the convergence speed. There is a lack of proper balance between exploration and exploitation phases. As the location of the best search is not considered a priority, therefore, it cannot jump out of the local optima, which represents a decline in performance.

If the vector position changes during the process, it might result in a larger step calculation and the search space not being explored properly. Correction factors $Cf_1$ and $Cf_2$ are introduced to minimise the change in vector position. The modified equations can be written as:

$$\vec{D} = \left|\vec{C}.\overrightarrow{X_{rand}} - \vec{X}\right| / Cf_1 \tag{13a}$$

$$\vec{X}(t+1) = \overrightarrow{X_{rand}} - \vec{X}.\vec{D} / Cf_1 \tag{14a}$$

The equation (14a) helps the whale survey the space of search efficiently in small steps and approach the prey. By modifying equation (12a), whales are made to swim in the shrunk space to catch their prey, thus enhancing the exploitation of the search space efficiently.

$$\vec{X}(t+1) = \vec{D}'.e^{bl}.\cos(2\Pi l) + \overrightarrow{X*}(t) / Cf_2 \tag{12a}$$

The exploration phase is also modified by the $Cf_2$ amount to limit the random movement of the whales. The values of $Cf_1$ and $Cf_2$ are 2.3 and 1.9, respectively. It was found that the whales reach the optimal solution in a search space efficiently and speedily compared to WOA. The steps followed to achieve the results are given as follows:

Step 1. Whales' population was initialized using $\overrightarrow{X_i}$ where, (i = 1, 2, 3, …, n)
Step 2. The values were updated for each search agent a, A, C, l, and p by using the condition (t < maximum iteration).
Step 3. For (p<0.5), if (|A| < 1), present search agent was updated using equation (7)
Step 4. If (|A| >=1), $\overrightarrow{X_{rand}}$ was selected and the present search agent was updated using equations (14a), (3), and (4)
Step 5. For (p>=0.5), the location of the present search agent was updated using equation (12a)
Step 6. If any search agent goes beyond the search space, then the process restarts from step 2.
Step 7. The fitness of each search agent and upgraded $\overrightarrow{X*}$ was computed. If the termination criteria are met, optimal solution (switching angles with the minimum corresponding THD) would be displayed otherwise process restarts from step 4.

## 5. PV-Wind characteristics equation

### *5.1 Wind turbine characteristics*

A wind turbine consists of blades that are fixed to the shaft through the gearbox and rotor hub. It transforms the kinetic energy to mechanical energy which is further converted to electrical energy by the shaft. The energy of the wind can be measured by $\rho$ is the air density, $v$ is the wind speed. The output mechanical power ($P_m$) achieved can be expressed as

$$P_m = \frac{1}{2}\rho A v^3 C_p(\lambda, \beta) \tag{15}$$

where, A is the swept area of the turbine, $C_p$ is the coefficient which judges the performance and also which is a non-linear function of Tip Speed Ratio (TSR), ($\lambda$) and pitch angle ($\beta$). TSR can be written as

$$\lambda = \frac{wR}{v} \tag{16}$$

where, $w$ is the speed of the turbine, R=radius of the blade.

$$C_p(\lambda, \beta) = C_1(C_2 / \lambda_i - C_3\beta - C_4)e^{-C_5/\lambda} \tag{17}$$

The value of ($C_1$, $C_2$, $C_3$, $C_4$) can be computed by estimating from the non-linear function or by the lookup table (Mahela et al. in 2018).

$$\lambda_i = \left[ \frac{1}{\lambda + .089} - \frac{0.035}{\beta^3 + 1} \right]^{-1} \tag{18}$$

The aim was to keep tracking the rotor speed with the changing wind velocity so that $C_p$ is set to the maximum value. To achieve maximum power from IG, $C_p$ should remain set to the highest value as shown in Fig. 3.

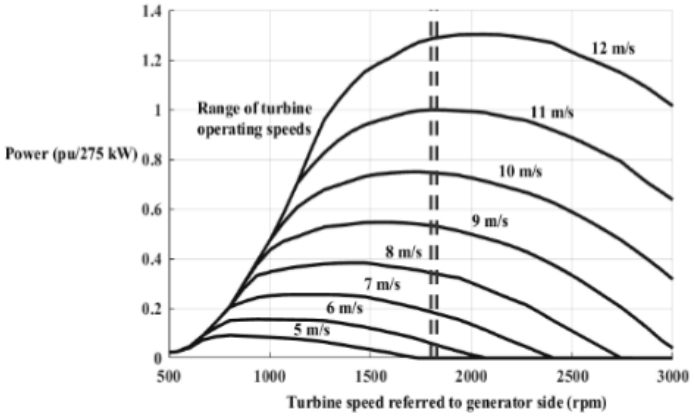


Fig. 3. Turbine power output versus speed of the shaft

### *5.2 Mathematical modeling of DFIG*

There are two categories of generators, comprising an induction generator and a synchronous generator. The present paper deals with the induction generator, which has three types: squirrel cage induction generator (SCIG), wound rotor induction generator (WRIG), and doubly fed induction generator (DFIG). Amongst all, DFIG is the most popular because of its simple pitch control, which deals with both active and reactive power. Besides this, it can work at variable speed, sub or synchronous speed to obtain maximum power as well. Power converters are much cheaper, lighter, and have less power loss as their ratings are only 30% of the power rating. The rating of DFIG can be observed in Table 1.

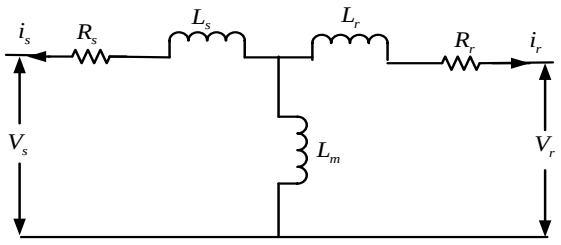


*a*

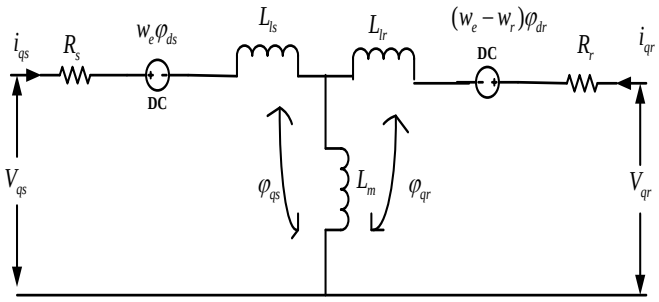


*b*

Fig. 4. DFIG (a) Equivalent circuit (b) Dynamic equivalent circuit in q axis frame

Equations (15)–(27) show the conventional equations for DFIG in a synchronous rotating frame. The equivalent circuit can be seen in the d and q axis frames in Fig. 4 and Fig. 5.

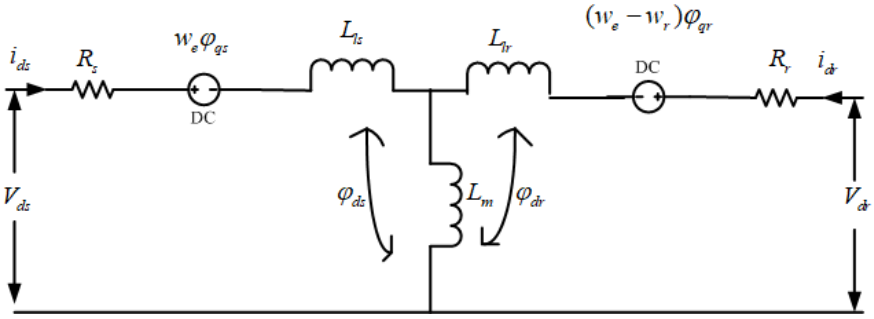


Fig. 5. Dynamic equivalent circuit in d axis frame

The d-q frame stator and rotor equations are given below.

$$V_{qs} = R_s i_{qs} + \frac{d}{dt}\varphi_{qs} + w_e\varphi_{ds} \tag{19}$$

$$V_{ds} = R_s i_{ds} + \frac{d}{dt}\varphi_{ds} + w_e\varphi_{qs} \tag{20}$$

$$V_{qr} = R_r i_{qr} + \frac{d}{dt}\varphi_{qr} + (w_e - w_r)\varphi_{dr} \tag{21}$$

$$V_{dr} = R_r i_{dr} + \frac{d}{dt}\varphi_{dr} + (w_e - w_r)\varphi_{qr} \tag{22}$$

Flux linkage equations can be written as

$$\varphi_{qs} = L_{ls} i_{qs} + L_m (i_{qs} + i_{qr}) \tag{23}$$

$$\varphi_{ds} = L_{ls} i_{ds} + L_m (i_{ds} + i_{dr}) \tag{24}$$

$$\varphi_{qr} = L_{lr} i_{qr} + L_m (i_{qs} + i_{qr}) \tag{25}$$

$$\varphi_{dr} = L_{lr} i_{dr} + L_m (i_{ds} + i_{dr}) \tag{26}$$

where, $V_{ds}$ ,$V_{qs}$, $V_{qr}$, $V_{dr}$, $\varphi_{ds}$, $\varphi_{qs}$, $\varphi_{dr}$, $\varphi_{qr}$, $i_{ds}$, $i_{dr}$,$i_{qs}$, $i_{qr}$, $L_{ls}$, $L_{lr}$, $R_s$, $R_r$ are the stator and rotor voltage, current, flux, difference of self-inductance and the mutual inductance and the resistance respectively, $L_m$ is the mutual inductance, $w_e$, $w_r$ are the angular and the rotor speed respectively. The active and reactive power of stator and rotor $P_s$, $Q_s$, $P_r$, $Q_r$ respectively can be written as:

$$P_s = \frac{3}{2}\left(V_{ds}i_{ds} + V_{qs}i_{qs}\right) \tag{27}$$

$$Q_s = \frac{3}{2}\left(V_{qs}i_{ds} - V_{ds}i_{qs}\right) \tag{28}$$

$$P_r = \frac{3}{2}\left(V_{dr}i_{dr} + V_{qr}i_{qr}\right) \tag{29}$$

$$Q_r = \frac{3}{2}\left(V_{qr}i_{dr} - V_{dr}i_{qr}\right) \tag{30}$$

By (31) electromagnetic torque ($T_{em}$) can be determined.

$$T_{em} = p(\varphi_{ds}i_{qs} - \varphi_{qs}i_{ds}) \tag{31}$$

where, p is no of pole pairs.

*Table 1*

**Ratings of the model used**

| **DFIG Specification** | | | | **Solar Panel Specifications** | | **Grid Specification** | |
|---|---|---|---|---|---|---|---|
| **Stator Parameters** | | **Rotor Parameters** | | | | | |
| Supply Voltage | 415 V | Rotor Voltage | 110 V | Voltage | 110 V | Grid voltage | 415 V |
| Stator frequency | 50 Hz | Resistance | 8 Ω | Rated power | 260 w | Frequency | 50 Hz |
| Power | 2.8 kw | Rotor speed | 1450 rpm | Open Circuit Voltage | 35.24 V | | |
| Inductance | 0.06 H | Inductance | 0.06 H | Short Circuit Current | 8.57 A | | |
| Resistance | 9 Ω | | | | | | |
| Mutual inductance | 0.79 H | | | | | | |

## 6. Results and discussion

The proposed model has been carried out in MATLAB 2016b. The angles for the inverters were found by the WOA. The five switching angles obtained for both the converters are

$\alpha_1 = 10.33^o$, $\alpha_2 = 18.16^o$, $\alpha_3 = 24.33^o$, $\alpha_4 = 25.07^o$, $\alpha_5 = 27.50^o$; $\alpha_1 = 16.33^o$, $\alpha_2 = 22.45^o$, $\alpha_3 = 23.45^o$, $\alpha_4 = 28^o$, $\alpha_5 = 32.47^o$, respectively for reducing the lower and

higher-order harmonics. These angles were stored in the lookup table offline for use later for online applications. The proposed control strategy has been used to get the outputs shown in Figures 6 and 7. The voltage waveforms at the stator and rotor sides are taken at a speed of 1450 rpm under both with and without harmonic elimination conditions.

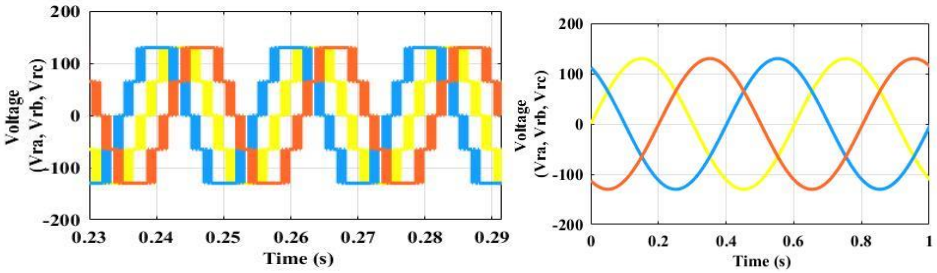


*a* *b*

Fig. 6. System output at 1450 rpm (a) rotor voltage output without harmonic elimination (b) rotor voltage output with harmonic elimination

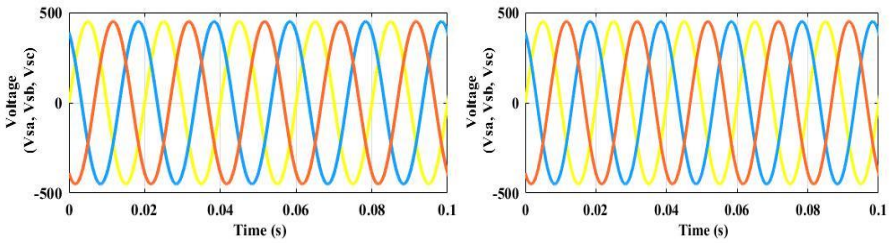


*a* *b*

Fig. 7. System output at 1450 rpm (a) stator output voltage without harmonic elimination (b) stator output voltage with harmonic elimination

By using the SHEPWM based MWOA control strategy, the pulses were generated at a modulation index of 0.85. The objective function equation (3) was used to get the optimized switching angles. Fig. 8 shows the different numbers of switching angles for n = 3, 5, and 7, over the range of modulation index. It was considered for up to twenty-nine harmonics. Higher orders can also be taken for testing the present system. For the computation of five switching angles, the $5^{th}$, 7th, $11^{th}$, $13^{th}$ harmonics, and fundamental were set to zero and the desired value, respectively. It was found that with just five switching angles, an equivalently good result was achieved with seven triggering pulses, keeping the system efficiency intact as well as keeping the switching losses low, as shown in Fig. 8. This means that with seven switching angles, the 5th, $7^{th}$, $11^{th}$, 13th, and $17^{th}$ can be controlled, but by using five triggering pulses, these lower orders can be controlled along with the higher orders like the $19^{th}$, $23^{rd}$, 25th, and 29th... etc. by using equation (3).

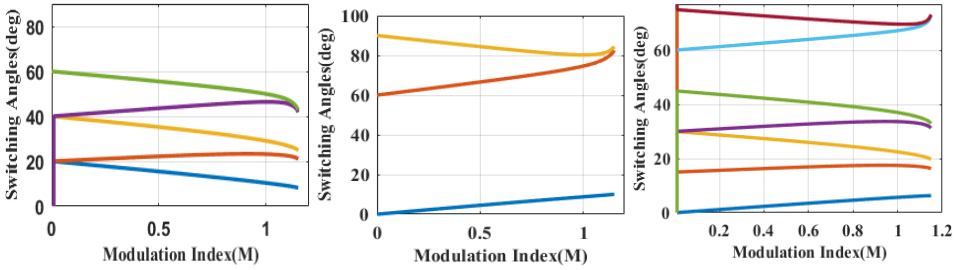


*a* *b* *c*

Fig. 8 Switching angles vs. modulation index (a) for five switching angles (b) for three switching angles (c) for seven switching angles

Fig. 9 (a) shows the THD variation over the modulation index for the different switching angles. The THD found by using different optimization algorithms at varying iterations is shown in Fig. 9 (b). It was discovered that using MWOA produces better results than other evolutionary techniques. The angles found when applying MWOA to the SHEPWM inverters are equally efficient in working as the seven switching angles, hence with reduced switching losses. The details of the parameters used have been given in Table 2. Harmonic spectra for various switching angles (n = 3, 5,7) at the rotor and stator side under with and without harmonics conditions have been shown in Fig. 10.

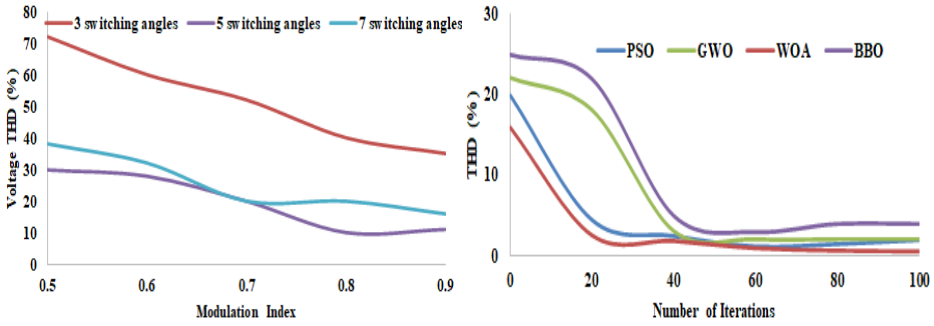


*a* *b*

Fig. 9. Characteristics behavior (a) THD vs. modulation index for various switching angles (b) THD vs. no. of iterations for various algorithms used

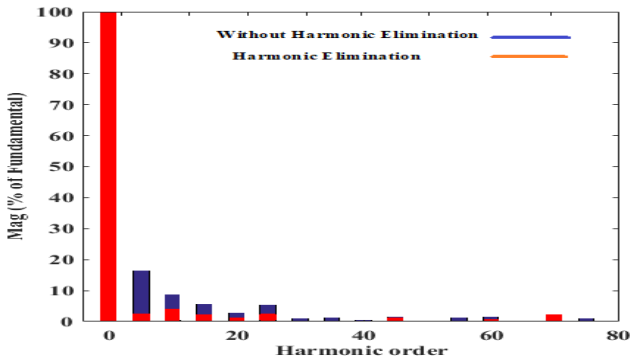


*a*

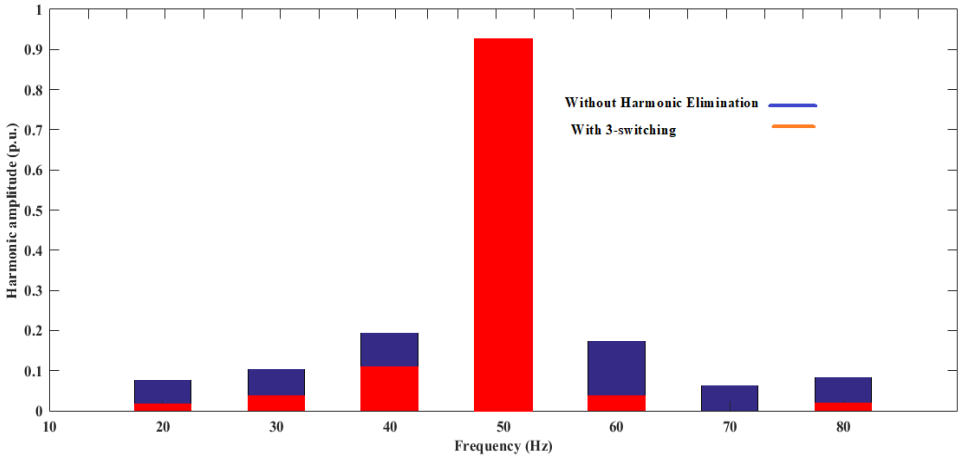


*b*

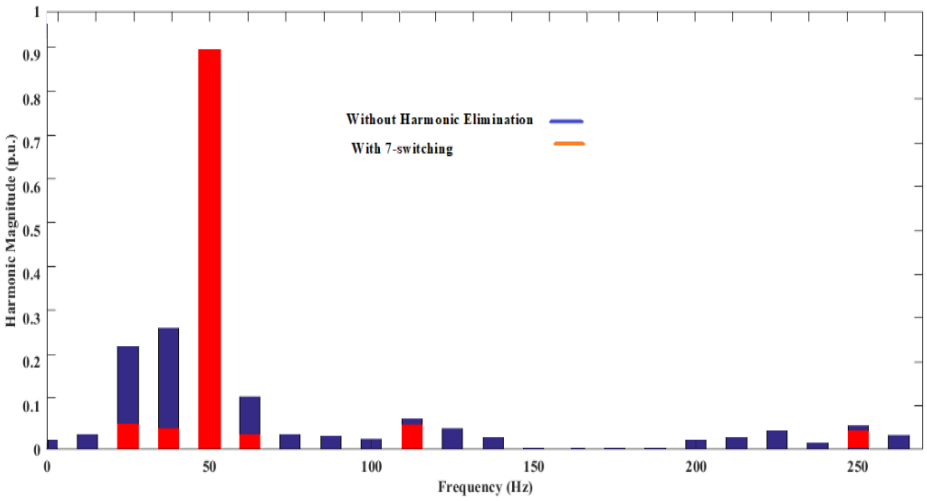


*c*

Fig. 10. DFIG harmonic spectra with and without harmonic (a) at rotor side (b) for three switching angles at stator side (c) for seven switching angles at stator side

*Table 2*

**Comparison of metaheuristic techniques with the proposed technique**

| **PSO** | | **MWOA** | | **GWO** | | **BBO** | |
|---|---|---|---|---|---|---|---|
| Weight (w) | 0.4 | Population matrix | 10*5 | Population matrix | 10*5 | Population size | 50 |
| Balance factors $c_1$, $c_2$, $c_3$, $c_4$ | 1.3,0.6, 1.9, 1.7 | | | | | Genes in each population | 5 |
| Random variable: $r_1$, $r_2$ | 0.6, 0.5 | Random variable $r_1$, $r_2$ | 0.7, 0.6 | Random variable $r_1$, $r_2$ | 0.7, 0.6 | Elitism value | 2 |
| No. of equations | Low | No. of equations | Low | No. of equations | Low | No. of equations | High |
| Complexity | Easy | Complexity | Easy | Complexity | Easy | Complexity | Moderate |
| CPU time (s) | 0.43 | CPU time (s) | 0.22 | CPU time (s) | 0.26 | CPU time (s) | 0.34 |
| THD (%) | 2.8 | THD (%) | 1.6 | THD (%) | 2.2 | THD (%) | 2.5 |

### *6.1 Experimental results*

A laboratory setup is shown in Fig. 11. The stator was coupled with the grid, and the rotor was fixed to the converter system. A set of insulated gate bipolar transistors (IGBT) was used, which were given the gate pulses from the microcontroller PIC18F452 based programmer. A driver circuit was made using TLP250H and it was powered by individual rectifier circuits.

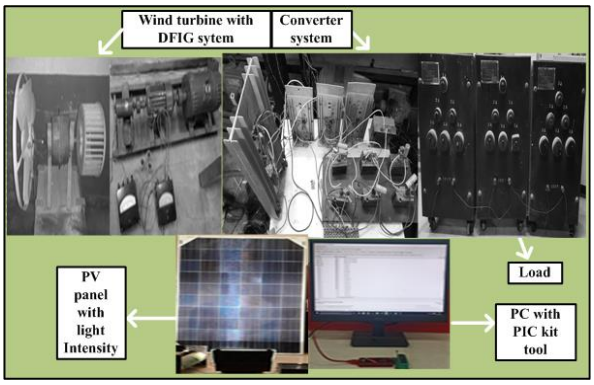


Fig. 11. Laboratory setup

A PV panel of 260W was used by VIKRAM Solar Company, powered by artificial insolation using incandescent bulbs. The outputs were observed on a Digital Storage Oscilloscope (DSO). The ratings used have been mentioned in Table 1.

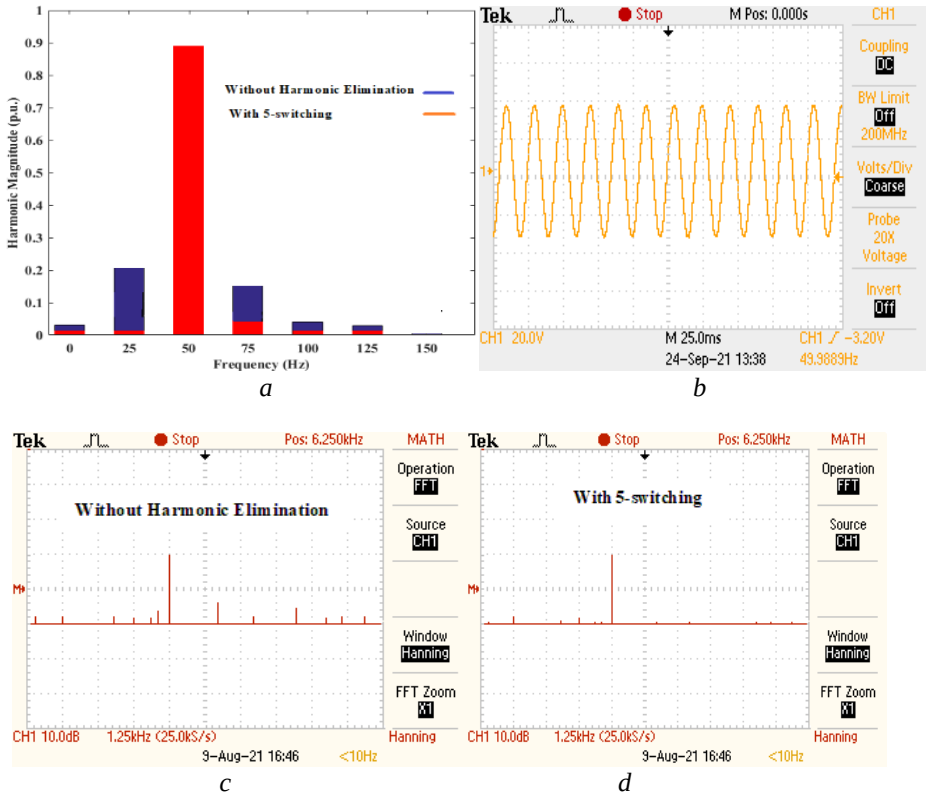


Fig. 12. Stator side FFT analysis for five switching's (a) FFT analysis in simulation (b) per phase voltage waveform at the stator side (channel 1: Y axis: 250V/div.) (c) experimental FFT analysis showing without harmonic elimination (d) experimental FFT analysis showing harmonic elimination

FFT analysis of the voltage at the stator side can be seen in Fig. 12 both for simulation and hardware model by applying the five angles obtained from MWOA in SHEPWM inverters. Hence, the software and experimental results obtained can be seen to be clearly in agreement. In the proposed technique, a load of 1.2 KVA was used at a power factor of 0.8 lag under before and after harmonic elimination conditions. In Table 3, a comparative analysis has been shown between the values of voltage harmonics deduced by $b_5$, $b_7$… of the standard reports and the proposed technique.

*Table 3*

**Comparison of voltage harmonic amplitudes of literature survey with the proposed technique**

| **Standard Reports used** | | | | | | | | | | |
|---|---|---|---|---|---|---|---|---|---|---|
| **Voltage harmonics amplitude on grid synchronisation** | **$b_5$** | **$b_7$** | **$b_{11}$** | **$b_{13}$** | **$b_{17}$** | **$b_{19}$** | **$b_{23}$** | **$b_{25}$** | **$b_{29}$** | **THD (%)** |
| **IEC 1996** | 5 | 4 | 3 | 2.5 | 1.6 | 1.2 | 1.2 | 1.2 | 1.06 | 6.5 |
| **CIGRE 2004** | 6 | 5 | 3.5 | 3 | 2 | 1.5 | 1.5 | 1.5 | -- | 8 |
| **Proposed Technique used** | | | | | | | | | | |

| **Voltage harmonics amplitude on grid synchronisation** | **$b_5$** | **$b_7$** | **$b_{11}$** | **$b_{13}$** | **$b_{17}$** | **$b_{19}$** | **$b_{23}$** | **$b_{25}$** | **$b_{29}$** | **THD (%)** |
|---|---|---|---|---|---|---|---|---|---|---|
| **Values** | 0.89 | 0.27 | 0.17 | 0.35 | 0.5 | 0.9 | 0.17 | 0.08 | 0.05 | 1.6 |

## 7. Conclusion

In the present paper, MWOA, BBO, PSO, and GWO-based inverters were used to reduce the lower and higher-order harmonics obtained at the stator and rotor side of the DFIG system. The best performance of all was that of MWOA, considering factors such as convergence time, minimum THD possible, etc. The angles obtained from the evolutionary techniques were stored offline in the microcontroller memory for online usage. Thus, with five switching angles, they achieve equivalently good results as seven switches. Thus, with fewer switching losses, system efficiency is maintained. A test system was also modelled to corroborate the simulation results for harmonics up to the 29$^{th}$ order. Various characteristic curves such as THD vs. iterations, THD vs. modulation index, etc. were carried out to justify the same. Thus, the proposed method achieves the desired purpose, and both the experimental and simulation results justify that it can be used for practical scenarios.

## R E F E R E N C E S

[1] Choudhary, P., and Srivastava, R. K. (2019) 'Sustainability perspectives-a review for solar photovoltaic trends and growth opportunities', Journal of Cleaner Production, Vol. 227, pp: 589-612.

[2] Ray, R. N., Chatterjee, D., & Goswami, S. K. (2009) 'Harmonics elimination in a multilevel inverter using the particle swarm optimization technique', IET Power Electronics, Vol. 2, No. 6, pp. 646-652.

[3] Elena, D. F., (2021) 'The impact of SVC device on the voltage and power quality in the electrical transmission network', U.P.B. Sci. Bull., series c, Vol. 83, Iss. 1, pp. 53-64, ISSN 2286-3540

[4] Ray, R.N., Chatterjee, D. and Goswami, S.K. (2010) 'A PSO based optimal switching technique for voltage harmonic reduction of multilevel inverter', Expert Syst. with Appl., Vol. 37, No. 12, pp.7796–7801.

[5] Tang, T., Han, J., & Tan, X. (2006) 'Selective harmonic elimination for a cascade multilevel inverter' In 2006 IEEE international symposium on industrial electronics, Vol. 2, pp. 977-981).

[6] Mahela, O. P., & Shaik, A. G. (2016) 'Comprehensive overview of grid interfaced wind energy generation systems' Renewable and Sustainable Energy Reviews, Vol. 57, pp. 260-281.

[7] Dris, Y., Benhabib, M.C., Meliani, S.M. & Dumbrava, V. (2021) 'Performance analysis of a hybrid farm (photovoltaic system wind turbine) connected to the grid using nine- switches converter', U.P.B. Sci. Bull., series c, Vol. 83, Iss. 3, pp. 53-64, ISSN 2286-3540.

[8] Bellabas, B., Denai, M. & Allaoui, T., (2020) 'A hierarchical control scheme to improve the stability and energy quality of a hybrid wind/photovoltaic system connected to the

electricity grid', U.P.B. Sci. Bull., series c, Vol. 82, Iss. 2, pp. 307-323, ISSN 2286-3540.
[9] Gao, K., Wang, T., Han, C., Xie, J., Ma, Y., & Peng, R. (2021) 'A Review of Optimization of Microgrid Operation', Energies, Vol. 14, No. 10, pp. 28-42.
[10] Sarker, K., Chatterjee, D., & Goswami, S. K. (2018) 'Modified harmonic minimisation technique for doubly fed induction generators with solar-wind hybrid system using biogeography-based optimisation, IET Power Electronics, Vol. 11, No. 10, pp. 1640-1651.
[11] Goud, B. S., & Rao, B. L. (2020) 'Power quality improvement in hybrid renewable energy source grid-connected system with grey wolf optimization, International Journal of Renewable Energy Research (IJRER), Vol.10, No. 3, pp.1264-1276.
[12] Routray, A., Singh, R. K., & Mahanty, R. (2019) 'Harmonic reduction in hybrid cascaded multilevel inverter using modified grey wolf optimization' IEEE Transactions on Industry Applications, Vol. 56, No. 2, pp.1827-1838.
[13] Wei, L., Li, K. & Wu, Y. (2021) 'Research on photovoltaic systems maximum power point tracking based on improved automatic Bacterial Foraging method', U.P.B. Sci. Bull., series C, Vol. 83, Iss. 3, ISSN 2286-3540.
[14] Rana, N., Abd Latiff, M. S., & Chiroma, H. (2020) 'Whale optimization algorithm: a systematic review of contemporary applications, modifications and developments' Neural Computing and Applications, pp. 1-33.
[15] Mohammed, H. M., Umar, S. U., & Rashid, T. A. (2019) 'A systematic and meta-analysis survey of whale optimization algorithm' Computational intelligence and neuroscience, 2019.
[16] Diab, A. A. Z., Sultan, H. M., Mohamed, I. S., Kuznetsov, O. N., & Do, T. D. (2019) 'Application of different optimization algorithms for optimal sizing of PV/wind/diesel/battery storage stand-alone hybrid microgrid', IEEE Access, Vol. 7, pp. 119223-119245.
[17] Ye, X., Liu, W., Li, H., Wang, M., Chi, C., Liang, G., ... & Huang, H. (2021) 'Modified Whale Optimization Algorithm for Solar Cell and PV Module Parameter Identification', Complexity, 2021.
[18] Youche L. & Huaizhong C. (2019) 'Optimization design for photovoltaic generation mppt based on improved adaptive genetic algorithm', U.P.B. Sci. Bull., series C, Vol. 81, Iss. 4.
[19] Chatterjee, D. (2011) 'A novel magnetizing-curve identification and computer storage technique for induction machines suitable for online application', IEEE Transactions on Industrial Electronics, Vol. 58, No. 12, pp. 5336-5343.
[20] CIGRE, J. W. (2004) C4. 07/CIRED 'Power quality indices and objectives', Final WG Report.
[21] International Electrotechnical Commission. (1996) 'Assessment of emission limits for distorting loads in MV and HV power systems', IEC technical report, 61000, pp. 3-6.